Journal of Applied Physics

Magnetic field and angle-dependent photoluminescence of a fiber-coupled nitrogen vacancy rich diamond

Cite as: J. Appl. Phys. **130**, 124901 (2021); https://doi.org/10.1063/5.0059330
Submitted: 08 June 2021 • Accepted: 06 September 2021 • Published Online: 23 September 2021

Ralf Wunderlich, Robert Staacke, Wolfgang Knolle, et al.

Journal of Applied Physics ARTICLE scitation.org/journal/jap

Magnetic field and angle-dependent photoluminescence of a fiber-coupled nitrogen vacancy rich diamond

Cite as: J. Appl. Phys. **130**, 124901 (2021); doi: 10.1063/5.0059330
Submitted: 8 June 2021 · Accepted: 6 September 2021 ·
Published Online: 23 September 2021

View Online Export Citation CrossMark

Ralf Wunderlich,[1,a)] Robert Staacke,[1] Wolfgang Knolle,[2] Bernd Abel,[2] and Jan Meijer[1]

AFFILIATIONS

[1]Faculty of Physics and Earth Sciences, Felix Bloch Institute for Solid State Physics, Leipzig University, Linnéstrasse 5, 04103 Leipzig, Germany
[2]Leibniz-Institute of Surface Engineering (IOM), Permoserstrasse 15, 04318 Leipzig, Germany

[a)]**Author to whom correspondence should be addressed:** ralf.wunderlich@uni-leipzig.de

ABSTRACT

Here, we investigate the magnetic field dependent photoluminescence (PL) of a fiber-coupled diamond single crystal with a high density of nitrogen vacancy (NV) centers. Angle-dependent magnetic field sweep measurements between 0 and 111 mT were performed using an oscillating illumination combined with lock-in techniques. Besides the expected superposed PL of differently oriented NV centers, a zoo of features in the PL are found. These features can be associated with level anti-crossings and cross relaxations. In particular, PL measurements allowed us to detect auto-cross relaxation between coupled NV centers. Moreover, the PL measurements at low magnetic fields show dips suggesting an interaction of NV centers with additional spin defects. The results presented here are not only a study for NV-based fiber-coupled sensors made of diamond, but also show a way to investigate with manageable effort and purely an optical multispin interaction with at least one NV center as a constituent.

INTRODUCTION

Diamond is the host material of one of the outstanding research objects in applied quantum physics in solids in the last decade—the negatively charged nitrogen vacancy defect center (NV center). This color center exhibits electronic spin polarization to its $|m = 0\rangle$ ground state under optical excitation[1] (see the supplementary material for the level scheme). This allows coherent control of individual electronic spins at room temperature with coherence times of a few milliseconds.[2] Thus, the exploration of fundamental quantum mechanical issues, such as entanglement, and the development of highly sensitive sensors based on quantum properties or nuclear hyperpolarization were achieved.[3–6] For example, such sensors have been used extensively for magnetic imaging of (anti-)ferromagnetic materials or for the study of skyrmions.[7–11] The conventional measurement principle for this is known as Optically Detected Magnetic Resonance (ODMR) and is based on the spin-dependent optical fluorescence of the NV center.[12,13] Measurements can be made on ensembles as well as on individual color centers. For the measurement of external fields, e.g., magnetic fields, it is advantageous to perform them on ensembles due to the higher signal-to-noise ratio ($SNR \sim \sqrt{n}$, n is the number of sensing spins). However, the indispensable use of microwaves, together with the associated equipment and experimental effort, makes this method complex and cost-intensive. In many cases, a simpler microwave-free method is much more cost–benefit efficient.

Due to an external magnetic field, a Zeeman splitting of the NV sublevels occurs. In general, this also results in mixing of these quantum mechanical spin states. This directly affects the intensity of the photoluminescence (PL) of the NV centers under optical excitation.[14] Accordingly, the magnetic field can be determined by measuring the PL intensity.[15–17] In contrast to a microwave based sensing scheme, sensitivity of this microwave-free approach is mainly limited by laser intensity noise, electronic noise, and the quality of the optical elements and fundamentally by the slope of the PL signal with the externally applied field. To take advantage of

ensemble measurements, here, the PL was studied on a red diamond that is extremely NV-rich. Here, a sample is said to be NV-rich if its PL shows a typical dip at about 59.5 mT, indicating an NV–NV interaction and thus a small average distance between NV centers (see the supplementary material).

All the revealed features in the magnetic field dependent PL of NV-rich diamonds, caused by spin state mixing, shed light on the quantum mechanical interactions of NV centers with their environment. Thus, ensemble measurements at high NV densities allow a systematic investigation at low defect-NV distances due to a high SNR. This is only possible to a limited extent for single measurements, e.g., with ODMR, since for statistical reasons, a defect pair, such as an NV–NV pair, would rarely be found. Thus, the measurements presented here are not only useful in the context of potential applications of NV-based magnetic field sensors but may contribute to the investigation of the defect-NV coupling for quantum information processing using coupled NV centers.[18,19] (While writing the paper, we became aware that the Budker group is working on a similar topic. The works are carried out independently.)

MATERIAL AND EXPERIMENTAL METHODS

The NV-rich sample is fabricated from a HPHT diamond with a high initial concentration of single substitutional nitrogen atoms. A large number of vacancies were created in the diamond sample using a 10 meV electron beam. In the process, the electron beam penetrates the millimeter-thick sample. One electron generates only a few vacancies ($\sim 3\,\mathrm{cm}^{-1}$), which thus have a large average distance. This reduces the probability of unwanted accumulations of vacancies. A high NV density can thus be achieved by simultaneous annealing. Here, the temperature (900 °C) is controlled by the beam current and the net vacancy density by the accumulated fluence of the irradiation ($2 \times 10^{18}\,\mathrm{cm}^{-2}$).[20] This process results in a mixture of substitutional nitrogen (P1) centers and NV centers in the sample. The defect concentrations in the studied diamond sample estimated by EPR measurements are [N] = 30 ppm and [NV] = 3 ppm, respectively.

The PL measurements were performed on a home-built setup (Fig. 1). As illumination source, we use a printed circuit board (PCB) with a laser diode (Osram Pl520B, 520 nm) including an electronic driver (icHaus iC-HKB). The magnetic field is generated by a cylindrical magnetic field system in which a two-axis rotator is located. The magnetic field system consists of three concentric cylindrical coils to achieve a large-scale homogeneous field and is connected to a power supply (EA PS 5000 A for fields up to 111 mT and R&S HMP2020 for sweeps below 50 mT). The diamond sample, about 2 mm in size, is attached to the end of a non-polarization-maintaining optical fiber (NA0.5, 400 μm core) and positioned goniometrically in the center of the magnetic field system. Laser light is coupled into the optical fiber to excite photoluminescence ($P_{\mathrm{exc}} \approx 25\,\mathrm{mW}$).[21–25] At the same time, it is used to collect the PL and direct it to a photodiode (Hamamatsu S5971) via a dichroic mirror (cut-on at 600 nm). The photodiode is mounted on another PCB together with amplifier electronics (simple transimpedance amplifier). To measure the voltage provided by the transimpedance amplifier, a lock-in amplifier (Zurich Instruments MFLI) was used. The laser and photodiode were

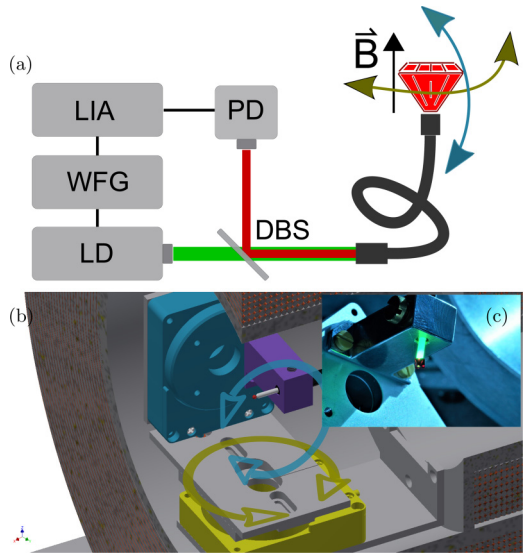

FIG. 1. (a) Sketch of the main parts of the setup consisting of a home-built laser source (LD) and a photodiode (PD) as a detector. The PD is connected to a lock-in amplifier (LIA). The pulsing of the laser was performed by a waveform generator (WFG), which also supplies the reference signal for the LIA. A dichroic beam splitter (DBS) is used to separate optical excitation and PL. (b) Illustration of the setup for the angle and magnetic field dependent PL measurements of the fiber-coupled diamond sample. It consists of two piezo-driven rotation stages (yellow, cyan) mounted in a home-built magnetic field coil system (gray-brown). An optical fiber (black) with a diamond (red) on its end is connected with the rotary stages via a holder (violet). The diamond sample is mounted goniomatically. (c) Photograph of the illuminated and mounted diamond sample.

supplied by a shielded 12 V battery to minimize noise. The pulsing of the laser was performed by a waveform generator (Keysight 33500B) at 375 and 250 kHz for the full magnetic field range scans, respectively. The dwell time for the PL measurement per magnetic field value ranged from 1 to 3 ms exclusive of a previous settling time for the magnetic field. Unless otherwise specified, the PL is normalized to the value without a magnetic field. In the following, the terminus "misalignment" is used as the angle relative to the ⟨111⟩ direction of the diamond lattice, and for "aligned" NV centers, it should always be assumed that their symmetry axis is parallel to the externally applied magnetic field.

RESULTS AND DISCUSSION

Figure 2(a) shows the PL over the entire investigated magnetic field range from 0 to 111 mT when the magnetic field is aligned with one of the four equivalent NV directions (<1°). As a comparison, the result from a simple model is shown, which calculates the PL of an ensemble of NV centers equally distributed on all directions in a diamond lattice at the corresponding magnetic field vector based on Ref. 14. The shape of the model curve results from the fact that when the sample is aligned with one NV direction along the external magnetic field, the three remaining NV

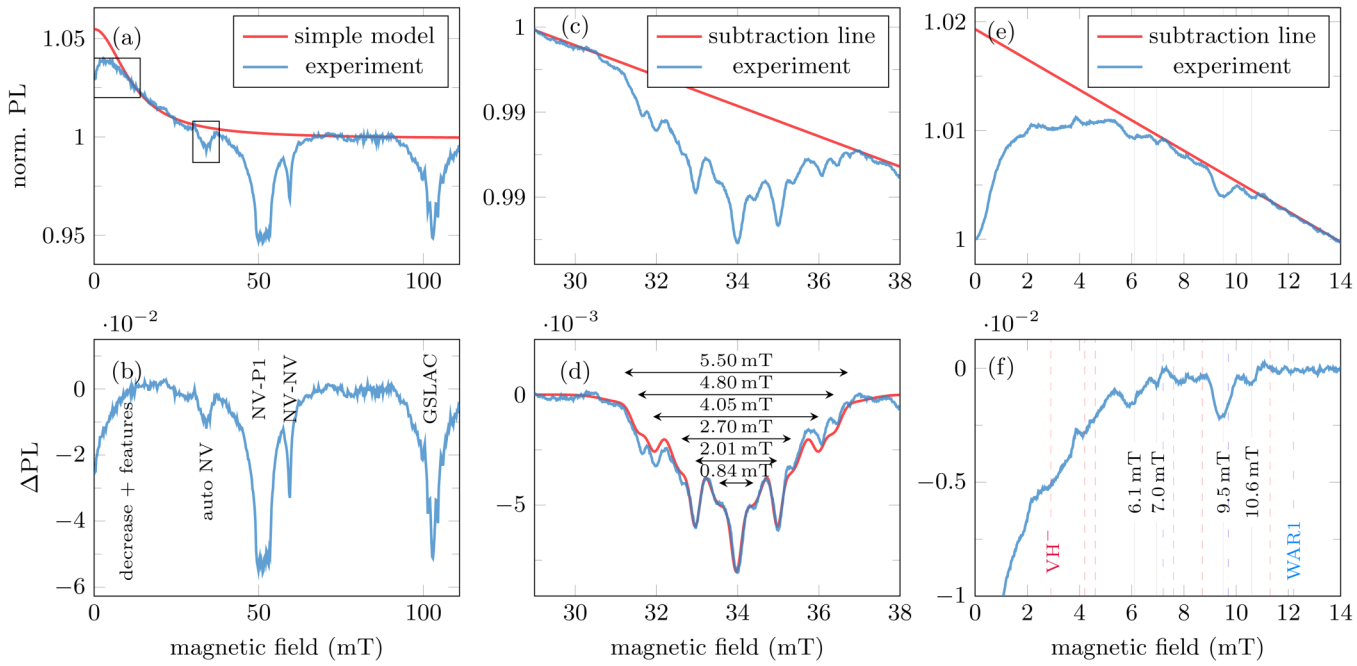

FIG. 2. (a) PL ($\vec{B} \parallel \langle 111 \rangle$) normalized to the plateau value around 80 mT (blue). The model (red) assumes an ensemble of NV centers in tetrahedral symmetry without coupling. (b) Difference of experimentally obtained data and model calculations from (a). (c) PL at ≈29–38 mT ($\vec{B} \parallel \langle 111 \rangle$) normalized to the value at 29 mT. (d) PL subtracted by the linear offset from (c) (blue), fitted by a symmetric multi-Gaussian function (red) with center at 34 mT. (e) PL from 0 to 14 mT ($\vec{B} \parallel \langle 111 \rangle$) normalized to the value at 0 mT. The red line shows a linear extrapolation of the PL, which is used as a subtraction line for the experimental data to visually clarify the resonance lines. (f) PL subtracted by the linear extrapolation shown in (e). Some of the most pronounced dips are indicated by vertical lines and magnetic field values. The dashed lines in red (dotted–dashed lines in blue) indicate the expected PL dips caused by CR of NV centers with nearby negatively charged VH^- centers (WAR1 centers).

directions are tilted by an angle of about 109° relative to the magnetic field vector according to tetragonal symmetry. For this sub-ensemble, this results in an increasing mixing of spin states with increasing magnetic field. Since this mixing determines the PL of an NV center, there is thus a decrease in PL with increasing magnetic field until, depending on the optical excitation power, saturation is reached. Briefly, the model shows the PL of an ensemble of undisturbed individual NV centers.[26] Obviously, the measured curve has some features that cannot be reproduced by this simple model. The difference between the model and the measurement is shown in Fig. 2(b). A pronounced drop (compared to the model curve) in the PL is seen at 0–10, 34, 51, 59.5, and 102 mT with some subtle substructures.

The feature at 102 mT can be assigned to the ground state level anti-crossing (GSLAC) of aligned NV centers.[27,28] According to the literature, the substructure is caused by coupling with neighboring ^{13}C spins.[15,29]

Since the conversion yield of P1 centers to NV centers is only in the low percentage range, there are also many NV–P1 pairs with a pairing distance below a threshold in which cross relaxation (CR) occurs. This takes place for aligned NV centers at about 51 mT. Due to the anisotropic hyperfine interaction of the electron spin of the P1 defect with its intrinsic nuclear nitrogen spin, the observed splitting of the PL dips results.[30–32]

With increasing NV density, the average distance between them decreases, and thus, a sub-ensemble that can no longer be neglected falls below a critical distance (a few nm) to a neighboring NV center. If only one of the two NV centers is aligned, CR between them occurs at about 59.5 mT, and therefore, the PL of the aligned NV center is reduced.[33] If the magnetic field is not perfectly aligned to an NV axis, three sub-ensembles of pairs with different angles relative to the aligned magnetic field result. Accordingly, this PL feature splits into three dips [e.g., see Fig. 4(a) for 3° misalignment].

Another configuration of an NV–NV pair exists when both constituents are aligned in the same direction; i.e., they are magnetically equivalent. Then, with an alignment along the magnetic field at about 34 mT, the three-spin state energy levels of the $^3A_2$ ground state become equally spaced.[34,35] However, CR of these two transitions ($|m\rangle : |0\rangle \leftrightarrow |1\rangle$ and $|-1\rangle \leftrightarrow |+1\rangle$) is forbidden since the spin is not conserved in this flip-flop process. The transition becomes allowed when the involved energy level functions change from pure states ($|0\rangle$, $|\pm 1\rangle$) to linear combinations of the triplet states. This happens, on the one hand, when the alignment of the NV centers no longer corresponds to that of the external magnetic field or, on the other hand, when a perturbation of the states, such as an interaction with at least one other spin, takes place. In the presented measurement, the alignment is better than 1°; therefore, the

observation of this PL feature can only be attributed to NV–NV CR, assuming sufficient dipole coupling between the two NV centers or an interaction with at least one other spin. Figure 2(c) shows a detailed scan of this feature. For an analysis of the splitting, we subtracted a linear background from the measured signal and fitted it with a symmetric multi-Gaussian function [Fig. 2(d)]. The similarity of the resonance structure with the GSLAC feature at 102 mT suggests that it is caused by an interaction with neighboring ^{13}C spins.[15]

In the following, we propose a simple model for the laser power dependence of this feature. Figure 3(a) shows a simulation of the laser power dependent level population of an individual NV center. Here, the term population is used as a synonym for occupation probability. Auto-CP between two NV centers involves the transition from level 1 to 2 for one NV center and from level 3 to 2 for the other. If we now assume the two NV centers to be a single system, the corresponding transition can be written as $|\text{level NV}_a \text{level NV}_b = 13\rangle \rightarrow |22\rangle$. This is shown in the inset in Fig. 3(b). Note here that the states are labeled with the levels, not with the magnetic quantum numbers. The decrease of PL at 34 mT can then be described by the population decrease of state $|13\rangle$ ($|$bright state, darker state) by auto-CR to state $|22\rangle$ ($|$darker state, darker state$\rangle$). For a fixed auto-CR rate (w_5), a factor p can be found that is proportional to the auto-CR probability and depends only on the population of the involved levels. For low to moderate laser powers, as used in this study, this proportional factor increases with increasing laser power according to the increasing population of level 1 for one NV center. In the range of very high laser powers, the probability for auto-CP decreases again due to the reduced population of the involved levels, e.g., pumping of the population in the excited and singlet state [Fig. 3(b)]; in other words, the PL feature is expected only at moderate laser powers so that only one of the two NV centers is polarized in the $|0\rangle$ ground state. Since we work with low laser powers, only the increase of the PL dip feature can be measured [Fig. 3(c)]. Details can be found in the supplementary material.

For the drop in the PL below 10 mT, dipolar coupling between neighboring NV centers ($d \lesssim 15$ nm) leading to mixing of spin states was proposed as an explanation.[36,37] However, a closer look reveals further substructures, which cannot be explained in this way [Fig. 2(e)]. We tried to reproduce these PL dips by different model calculations such as CR of NV − P1, NV − NV, and NV − (NV + P1) or even between the negative and neutral charge state of the NV center ($\text{NV}^- - \text{NV}^0$). None of the models could satisfactorily explain the observed resonances at low magnetic fields ($B < 14$ mT). Also, the LACs caused by the interaction of the electron spin of the NV center and its intrinsic nuclear nitrogen spin in combination with a small transverse magnetic field (In our case, this is true for the sub-ensemble of NV centers not with their symmetry axis parallel to $\vec{B}$.) cannot explain the observed features.[38] As recently proposed for the PL of CVD-grown diamond samples, we investigate the potential CR with negatively charged VH^- centers and WAR1 centers.[39] The corresponding magnetic fields are indicated in Fig. 2(f) with red dashed (blue dotted–dashed) vertical lines for the VH^- center (WAR1 center). While some of the PL dips could possibly be attributed to these defects, there are also some that cannot be explained in this way (e.g., the 6.1 mT dip among others). Details can be found in the supplementary material. For HPHT diamonds, an iron, nickel, or cobalt related defect would be more likely since these elements are used as catalysts in the growth process.[40] These defect centers mostly have a spin

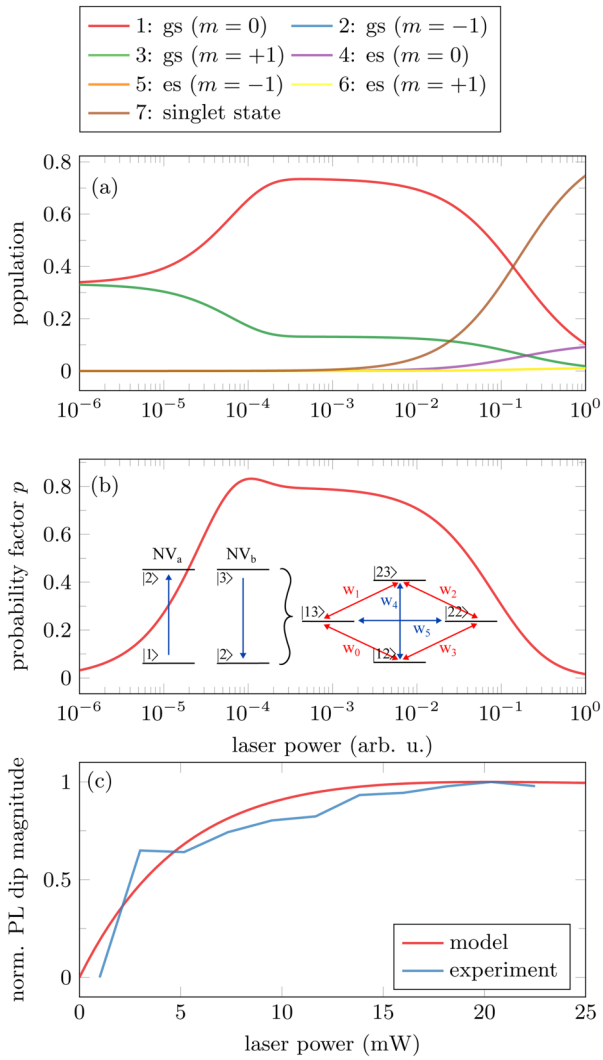

FIG. 3. (a) Simulation of the laser power dependent population of an NV center after 1 ms in a seven level model (levels denoted as given in the supplementary material). Note that levels 2 and 3 as well as levels 5 and 6 are degenerated since the magnetic field is aligned along the ⟨111⟩ direction. (b) Probability factor p for auto-CP of two coupled NV centers (NV_a and NV_b in the inset) at 34 mT. The left side of the inset depicts the involved levels for this process (1 and 2 for NV_a and 2 and 3 for NV_b). The right side of the inset depicts the four level model (level NV_a and level NV_b) with the corresponding transition probabilities w. Auto-CP occurs between the state $|13\rangle$ and $|22\rangle$ (w_5). Note here that the states are denoted by the levels, not by the magnetic quantum numbers. (c) The laser power dependent magnitude of the PL dip at 34 mT compared to the scaled values of the model. Below 1 mW, no PL dip can be observed. Note that (a) and (b) are plotted in a logarithmic scale and (c) in a linear scale.

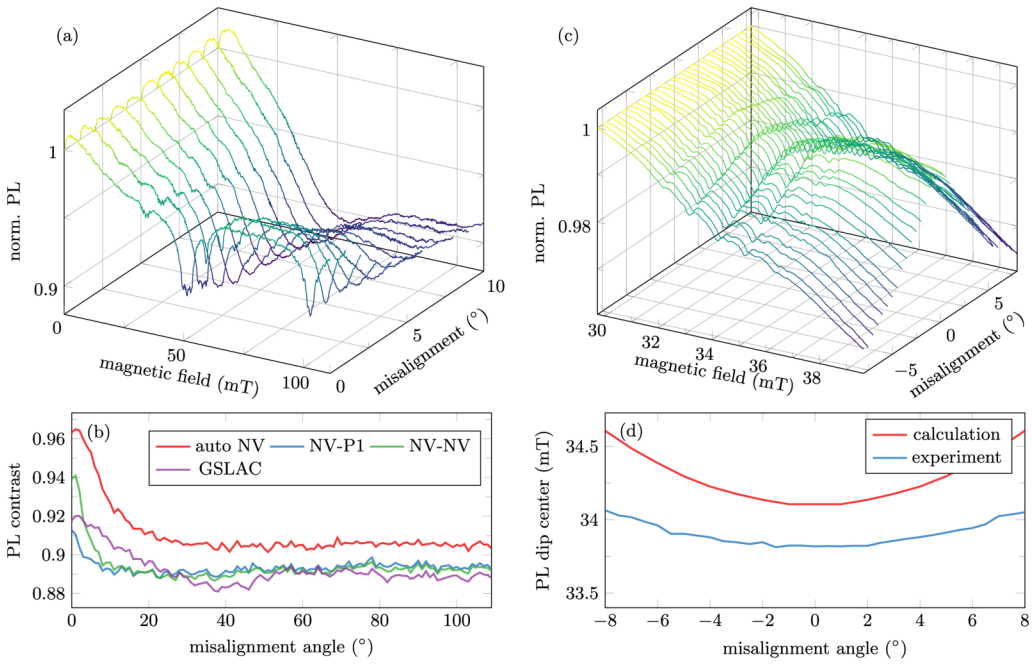

FIG. 4. Angle-dependent PL measurements for 0–111 mT (a) and 30–39 mT (c). From these data, the angle-dependent PL contrast for different PL features can be extracted (c). (d) Calculated and measured magnetic field position for the PL dip caused by NV auto-CR.

$S = 1/2$, which cannot explain the observed PL dips in this magnetic field region.[41–44] However, supposing that the observed PL dips are caused by CR, one should assume that it is caused by a defect center with a zero-field splitting (ZFS). The Ni-related center AB5 has a spin of $S = 1$, but with a ZFS of about 32 GHz along the $\langle 111 \rangle$ axis, it has a value more than one order of magnitude above that of the NV center and, therefore, cannot explain the observed dips either.[45] Thus, the origin of these PL features remains unknown at present.

Figures 4(a) and 4(c) show a set of PL measurements for different magnetic field ranges at varying misalignment angles. Figure 4(a) shows a section (0°–10°) from a series of measurements of misalignment angles up to 109° in 1° steps (full measurement in the supplementary material). As the angle increases, the features described above become less pronounced. The angle-dependent PL contrast of the various PL features relative to $\mathrm{PL}(B = 0)$ was also extracted from the full measurement series and is shown in Fig. 4(b). The PL contrast decreases rapidly with increasing misalignment, which can be attributed to mixing of the spin states of the initially aligned NV centers.

For the magnetic field region around 34 mT where auto-CP of the NV centers occurs, detailed measurements from an −8° to +8° tilt angle were recorded [Fig. 4(c)]. The exact magnetic field position of this feature was then extracted. For this purpose, a symmetric multi-Gaussian function was fitted to the curve for each magnetic field scan [compare Fig. 2(d)], and the resulting position was plotted as a function of the angle [Fig. 4(d)]. A comparison with numerically calculated values for the dip position shows a basic agreement in the curve shape. However, the calculated value of the magnetic field position deviates by 0.3 mT from the measured one, and also, the curvature of the curves does not match exactly. The reason for this could be that the calculation did not include coupling with additional spins, such as ^{13}C spins. Furthermore, it is known that strong internal stress can occur in diamonds, leading to a shift of the energy levels, and thus also of the energetic resonances leading to the CR. Due to the geometry and optical absorption of the sample, it is not possible to perform optical cross-polarization measurements that could indicate internal stress; therefore, we cannot rule this out in the measured sample.

CONCLUSION AND OUTLOOK

An NV-rich diamond was created by electron irradiation and attached to the end of an optical fiber. By a lock-in technique, the PL could be recorded angle dependent at magnetic fields between 0 and 111 mT. This revealed couplings with different neighboring spins by comparison with a PL model for an ensemble of individual NV centers. In addition to the GSLAC and coupling with neighboring P1 centers, coupling among NV centers could also be detected. By choosing moderate irradiation powers, the coupling of magnetically equivalent NV centers could be shown in addition to that of magnetically in-equivalent ones.

Moreover, the measurements show a possibility to study paramagnetic defects in diamond in general. For the magnetic field region below about 10 mT, further dips appear in the PL measurements. These PL dips were compared with literature values.

However, no simple model involving the spin defects discussed in the text could be found to reproduce every PL dip. In future studies, the PL features should be systematically related to the concentration of impurities. These could be determined, for example, by EPR or PIXE. Moreover, multispin interactions should not be excluded as the origin of the unexplained PL features. In particular, the possibility of studying three-spin coupling between NV–NV–P1 or NV–P1–P1 potentially arises at very high NV densities.

SUPPLEMENTARY MATERIAL

See the supplementary material that provides details on the setup, sample properties, and calculations.

ACKNOWLEDGMENTS

This work was supported by the EU–FET Flagship on Quantum Technologies through the Project ASTERIQS, through the QUANTERA project MICROSENS, and through the BMBF joint project DiaQuantFab. We acknowledge support from the Leipzig University within the program of Open Access Publishing.

DATA AVAILABILITY

The data that support the findings of this study are available from the corresponding author upon reasonable request.

REFERENCES

[1]G. M. H. Thiering and A. Gali, Phys. Rev. B **98**, 085207 (2018).
[2]N. Bar-Gill, L. Pham, A. Jarmola, D. Budker, and R. Walsworth, Nat. Commun. **4**, 45 (2013).
[3]D. R. Glenn, D. B. Bucher, J. Lee, M. D. Lukin, H. Park, and R. L. Walsworth, Nature **555**, 351 (2018).
[4]G. Balasubramanian, I. Y. Chan, R. Kolesov, M. Al-Hmoud, J. Tisler, C. Shin, C. Kim, A. Wojcik, P. R. Hemmer, A. Krueger, T. Hanke, A. Leitenstorfer, R. Bratschitsch, F. Jelezko, and J. Wrachtrup, Nature **455**, 648 (2008).
[5]T. Wolf, P. Neumann, K. Nakamura, H. Sumiya, T. Ohshima, J. Isoya, and J. Wrachtrup, Phys. Rev. X **5**, 041001 (2015).
[6]R. Wunderlich, J. Kohlrautz, B. Abel, J. Haase, and J. Meijer, Phys. Rev. B **96**, 220407 (2017).
[7]B. A. McCullian, A. M. Thabt, B. A. Gray, A. L. Melendez, M. S. Wolf, V. L. Safonov, D. V. Pelekhov, V. P. Bhallamudi, M. R. Page, and P. C. Hammel, Nat. Commun. **11**, 453 (2020).
[8]S. Fu, K. Kang, K. Shayan, A. Yoshimura, S. Dadras, X. Wang, L. Zhang, S. Chen, N. Liu, A. Jindal, X. Li, A. N. Pasupathy, A. N. Vamivakas, V. Meunier, S. Strauf, and E.-H. Yang, Nat. Commun. **11**, 777 (2020).
[9]A. Finco, A. Haykal, R. Tanos, F. Fabre, S. Chouaieb, W. Akhtar, I. Robert-Philip, W. Legrand, F. Ajejas, K. Bouzehouane, N. Reyren, T. Devolder, J.-P. Adam, J.-V. Kim, V. Cros, and V. Jacques, Nat. Commun. **12**, 231 (2021).
[10]F. Fabre, A. Finco, A. Purbawati, A. Hadj-Azzem, N. Rougemaille, J. Coraux, I. Philip, and V. Jacques, Phys. Rev. Mater. **5**, 034008 (2021).
[11]I. Gross, W. Akhtar, A. Hrabec, J. Sampaio, L. J. Martínez, S. Chouaieb, B. J. Shields, P. Maletinsky, A. Thiaville, S. Rohart, and V. Jacques, Phys. Rev. Mater. **2**, 024406 (2018).
[12]E. van Oort, N. B. Manson, and M. Glasbeek, J. Phys. C: Solid State Phys. **21**, 4385 (1988).
[13]P. Delaney, J. C. Greer, and J. A. Larsson, Nano Lett. **10**, 610 (2010).
[14]J.-P. Tetienne, L. Rondin, P. Spinicelli, M. Chipaux, T. Debuisschert, J.-F. Roch, and V. Jacques, New J. Phys. **14**, 103033 (2012).
[15]A. Wickenbrock, H. Zheng, L. Bougas, N. Leefer, S. Afach, A. Jarmola, V. M. Acosta, and D. Budker, Appl. Phys. Lett. **109**, 053505 (2016).
[16]R. Staacke, R. John, R. Wunderlich, L. Horsthemke, W. Knolle, C. Laube, P. Glösekötter, B. Burchard, B. Abel, and J. Meijer, Adv. Quantum Technol. **3**, 2000037 (2020).
[17]H. Zheng, Z. Sun, G. Chatzidrosos, C. Zhang, K. Nakamura, H. Sumiya, T. Ohshima, J. Isoya, J. Wrachtrup, A. Wickenbrock, and D. Budker, Phys. Rev. Appl. **13**, 044023 (2020).
[18]F. Dolde, I. Jakobi, B. Naydenov, N. Zhao, S. Pezzagna, C. Trautmann, J. Meijer, P. Neumann, F. Jelezko, and J. Wrachtrup, Nat. Phys. **9**, 139 (2013).
[19]M. W. Doherty, C. A. Meriles, A. Alkauskas, H. Fedder, M. J. Sellars, and N. B. Manson, Phys. Rev. X **6**, 041035 (2016).
[20]Y. Mindarava, R. Blinder, C. Laube, W. Knolle, B. Abel, C. Jentgens, J. Isoya, J. Scheuer, J. Lang, I. Schwartz, B. Naydenov, and F. Jelezko, Carbon **170**, 182 (2020).
[21]S. M. Blakley, I. V. Fedotov, S. Y. Kilin, and A. M. Zheltikov, Opt. Lett. **40**, 3727 (2015).
[22]I. V. Fedotov, S. M. Blakley, E. E. Serebryannikov, P. Hemmer, M. O. Scully, and A. M. Zheltikov, Opt. Lett. **41**, 472 (2016).
[23]D. Duan, G. X. Du, V. K. Kavatamane, S. Arumugam, Y.-K. Tzeng, H.-C. Chang, and G. Balasubramanian, Opt. Express **27**, 6734 (2019).
[24]D. Bai, M. H. Huynh, D. A. Simpson, P. Reineck, S. A. Vahid, A. D. Greentree, S. Foster, H. Ebendorff-Heidepriem, and B. C. Gibson, APL Mater. **8**, 081102 (2020).
[25]D. Duan, V. K. Kavatamane, S. R. Arumugam, Y.-K. Tzeng, H.-C. Chang, and G. Balasubramanian, Appl. Phys. Lett. **116**, 113701 (2020).
[26]R. J. Epstein, F. M. Mendoza, Y. K. Kato, and D. D. Awschalom, Nat. Phys. **1**, 94 (2005).
[27]X.-F. He, N. B. Manson, and P. T. H. Fisk, Phys. Rev. B **47**, 8809 (1993).
[28]L. J. Rogers, R. L. McMurtrie, M. J. Sellars, and N. B. Manson, New J. Phys. **11**, 063007 (2009).
[29]V. Ivády, H. Zheng, A. Wickenbrock, L. Bougas, G. Chatzidrosos, K. Nakamura, H. Sumiya, T. Ohshima, J. Isoya, D. Budker, I. A. Abrikosov, and A. Gali, Phys. Rev. B **103**, 035307 (2021).
[30]W. V. Smith, P. P. Sorokin, I. L. Gelles, and G. J. Lasher, Phys. Rev. **115**, 1546 (1959).
[31]K. Holliday, N. B. Manson, M. Glasbeek, and E. van Oort, J. Phys.: Condens. Matter **1**, 7093 (1989).
[32]R. Lazda, L. Busaite, A. Berzins, J. Smits, F. Gahbauer, M. Auzinsh, D. Budker, and R. Ferber, Phys. Rev. B **103**, 134104 (2021).
[33]S. Armstrong, L. J. Rogers, R. L. McMurtrie, and N. B. Manson, Phys. Procedia **3**, 1569 (2010).
[34]E. van Oort and M. Glasbeek, Phys. Rev. B **40**, 6509 (1989).
[35]E. van Oort and M. Glasbeek, Appl. Magn. Reson. **2**, 291 (1991).
[36]S. V. Anishchik, V. G. Vins, A. P. Yelisseyev, N. N. Lukzen, N. L. Lavrik, and V. A. Bagryansky, New J. Phys. **17**, 023040 (2015).
[37]R. Akhmedzhanov, L. Gushchin, N. Nizov, V. Nizov, D. Sobgayda, I. Zelensky, and P. Hemmer, Phys. Rev. A **96**, 013806 (2017).
[38]H. Clevenson, E. H. Chen, F. Dolde, C. Teale, D. Englund, and D. Braje, Phys. Rev. A **94**, 021401 (2016).
[39]C. Pellet-Mary, P. Huillery, M. Perdriat, A. Tallaire, and G. Hétet, Phys. Rev. B **103**, L100411 (2021).
[40]K. Iakoubovskii, Phys. Rev. B **70**, 205211 (2004).
[41]V. A. Nadolinny, A. P. Yelisseyev, O. P. Yuryeva, and B. N. Feygelson, Appl. Magn. Reson. **12**, 543 (1997).
[42]K. Johnston, A. Mainwood, A. T. Collins, G. Davies, D. Twitchen, J. Baker, and M. Newton, Physica B **273–274**, 647 (1999).
[43]V. A. Nadolinny, A. P. Yelisseyev, J. M. Baker, M. E. Newton, D. J. Twitchen, S. C. Lawson, O. P. Yuryeva, and B. N. Feigelson, J. Phys.: Condens. Matter **11**, 7357 (1999).
[44]V. A. Nadolinny, J. M. Baker, O. P. Yuryeva, M. E. Newton, D. J. Twitchen, and Y. N. Palyanov, Appl. Magn. Reson. **28**, 365 (2005).
[45]A. Neves, R. Pereira, N. Sobolev, M. Nazaré, W. Gehlhoff, A. Näser, and H. Kanda, Diam. Relat. Mater. **9**, 1057 (2000).